ELSEVIER

Journal of Biomechanics 41 (2008) 2446–2457

JOURNAL OF BIOMECHANICS

www.elsevier.com/locate/jbiomech
www.JBiomech.com

Numerical investigation of the three-dimensional flow in a human lung model

Rainhill K. Freitas*, Wolfgang Schröder

RWTH Aachen University, Institute of Aerodynamics, Wüllnerstr. 5a, 52062 Aachen, Germany

Accepted 15 May 2008

Abstract

The flow field at inspiration and expiration in the upper human airways consisting of the trachea down to the sixth generation of the bronchial tree is numerically simulated. The three-dimensional steady flow at a hydraulic diameter-based Reynolds number $Re_D = 1250$ is computed via a lattice-Boltzmann method (LBM). The simulation is validated by the experimental data based on particle-image velocimetry (PIV) measurements. The good agreement between numerical and experimental results is evidenced by comparing velocity contours and distributions in a defined reference plane. The results show the LBM to be an accurate tool to numerically predict flow structures in the human lung. Using an automatic Cartesian grid generator, the overall process time from meshing to a steady-state solution is <12 h. Moreover, the numerical simulation allows a closer analysis of the secondary flow structures than in the experimental investigation. The three-dimensional streamline patterns reveal some insight on the air exchange mechanism at inspiration and expiration. At inspiration, the slower near-wall tracheal flow enters through the right principal bronchus into the right upper lobar bronchus. The bulk mass flux in the trachea is nearly evenly distributed over the left upper, center and lower lobar bronchi and the right center and lower bronchi. At expiration, the air from the right upper lobar bronchus enters the right center of the trachea and displaces the airflow from the lower and center right bronchi such that the tracheal positions of the streamlines at inspiration and expiration are switched. The flow in the left bronchi does not show this kind of switching. The findings emphasize the impact of the asymmetry of the lung geometry on the respiratory air exchange mechanism.

Keywords: Lattice Boltzmann; Human lung cast; Human airways; Respiratory flow simulation

1. Introduction

The study of air exchange processes in the human respiratory system plays an important role in medicine and biomedical engineering. Major interests of investigations in this field concern aerosolized drug delivery, pulmonary disease diagnostics and high-frequency ventilation (HFV) phenomena. While the chemical processes and the general function of the respiratory system are well understood, the correct fluid mechanical description of the gas exchange process remains a challenge. This is due to the fact that the human lung has an extremely complex asymmetric and irregular shape varying substantially per individual.

Therefore, most of the investigations are based on simplified models of the essential structures in the lung, i.e., the first few generations of the bronchial tree. The most popular of these models is the Weibel model by Weibel (1963), which describes the bronchi as a symmetric tree structure of subsequent bifurcating tubes with 23 generations. However, instead of the full-scale three-dimensional model, usually, only the first 3–5 generations are considered and a planar representation is often favored for simplicity.

To obtain a more realistic configuration an additional geometrical description of the bifurcation topology is often applied, which ensures a smooth transition from parent to daughter tube.

Detailed experimental studies of the steady inspiratory and expiratory flow through a planar symmetric bifurcation have been performed by Zhao and Lieber (1994a, b).

*Corresponding author. Tel.: +49 241 809 4820.
E-mail address: r.freitas@aia.rwth-aachen.de (R.K. Freitas).

0021-9290/$ - see front matter © 2008 Elsevier Ltd. All rights reserved.
doi:10.1016/j.jbiomech.2008.05.016

Their experiments describe some fundamental flow phenomena in the lung like counter-rotating vortices and an M-shaped velocity profile for expiratory flow in the main branch. However, the effect of three-dimensional bifurcation structures, a non-smooth surface and, as the authors also point out, the impact of successive bifurcations and asymmetric branching are neglected in the measurements.

Simulations for the planar Weibel model with physically realistic bifurcations were performed, e.g., by Zhang et al. (2002). Flow field investigations with a non-planar Weibel model were conducted by several researchers. For instance, Nowak et al. (2003), who compared the results for the Weibel model and a computer tomography (CT)-based model and, Comer et al. (2001), who found significant differences in the flow field for planar and non-planar models. More realistic geometries include the consideration of asymmetric bifurcations by Liu et al. (2003), cartilage ring structures in the trachea by Li et al. (2007), and CT-based models by Nowak et al. (2003), Ertbruggen et al. (2005) and Lin et al. (2007). In all these studies, the importance of realistic models has been emphasized. As stated in Nowak et al. (2003) a substantial prediction of the flow field in a real world human lung can only be obtained from a "true geometry" which today is the best approximated by CT data or an actual human lung cast.

Besides the realism of the geometry there are additional influences on the accuracy of numerical simulations, like the applied numerical method, the computational resolution and the boundary conditions. Therefore, it will always be necessary to validate numerical by experimental data. On the other hand, the basic validation hypothesis is assumed that a simulation setup which gives good results for a certain flow problem also will deliver reasonable results for a similar flow problem, i.e., a flow with only slightly different parameters and likewise boundary conditions.

The objective of this study is threefold. Firstly, the LBM will be shown to be an appropriate method to investigate the flow field in the respiratory system with special advantages concerning the grid generation process and the overall computational time. Secondly, the numerical simulation results allow an extended analysis of the three-dimensional flow structures, which have been observed in the experiments by Große et al. (2007). Finally, through the detailed visualization of the complete three-dimensional data set general airflow patterns are identified, yielding a better understanding of the fundamental exchange mechanism in the respiratory system.

The article possesses the following structure. In the following section the simulation setup is described, consisting of a short overview of the numerical method, the applied boundary conditions and the computational grid generation process. The numerical and experimental findings are juxtaposed in the subsequent section. Then, the intricate three-dimensional flow patterns are discussed with emphasis on the exchange mechanisms and finally, some conclusions are drawn along with a brief outlook.

2. Simulation setup

2.1. Lattice-Boltzmann method (LBM)

The LBM constitutes a special solution algorithm for isothermal continuum flows in the low Mach number and moderate Reynolds number regime. The basic variant of the LBM is based on the Boltzmann equation with a simplified right-hand side, i.e., collision term, as proposed by Bhatnagar, Gross, and Krook (BGK), Bhatnagar et al. (1954). It has been shown in the literature, (Hänel, 2004), that the LBM solves indeed the Navier–Stokes equations. There are some often mentioned advantages of the LBM over, e.g., finite-difference and finite-volume methods like the capability to efficiently describe multi-phase flows, its low-computational costs, very good parallel scale-up and a very efficient boundary treatment for fixed walls, i.e., the flow in extremely intricate geometries can be efficiently investigated. Besides these favorable features the method still possesses some drawbacks, which aggravate the method's application namely in high Reynolds number flows, due to its complex stability behavior. That is, the stability depends non-linearly on the viscosity, the local velocity, the grid resolution and the formulation of the boundary conditions.

Moreover, the choice of non-solid wall boundary conditions is not straightforward due to the underlying particle distribution function discretization of the LBM. In other words, the transformation of macroscopic flow variables, which are prescribed on the inflow boundaries, into distribution functions is not unique. Note, the Mach and Reynolds number ranges in the upper human airways are safely within the stability ranges of nearly all variants of the LBM especially the BGK method, such that only the correct choice of boundary conditions and a sufficiently high-grid resolution have to be provided. The applied Mach number is much lower than the stability boundary of the LBM (between 0.1 and 0.2) and accordingly the flow can be considered incompressible.

It goes without saying, that a lot of research,(d'Humieres et al., 2002; Geier et al., 2006; Boghosian et al., 2001) has been devoted towards more stable LBMs. However, despite the success of these advanced methods in certain areas of application the improved stability behavior is yet to be shown for general complex flows, whereas the BGK method is known to deliver stable and accurate results for quite a range of varying flows. This has been shown by Freitas and Schröder (2008) and Geller et al. (2006).

Recently, the LBM–BGK method has also been applied to investigate the flow through an idealized upper human airway by Ball et al. (2007) and for the simulation of the flow through the nasal cavity by Finck et al. (2007). In other words, this method has already been shown to yield accurate and physically meaningful results in comparable with biomedical problems.

In the following, a brief description of the LBM based on the BGK approximation is given. The BGK equation describes the evolution of a molecular distribution function

in the phase space, which is the superposition of a Euclidian space and a velocity space. In the present work the D3Q19 model has been applied. The D*n*Q*m* notation, in which n stands for the number of dimensions and m stands for the number of discrete velocities, has been introduced by Qian et al. (1992), where also a detailed discussion on other valid phase space discretizations can be found. The numbering of the discrete velocity set for this model is shown in Fig. 1. It reads

$$\xi_i = \delta x/\delta t \begin{cases} (0,0,\mp 1);(0,\mp 1,0);(\mp 1,0,0), & \alpha = 0..5 \\ (\mp 1,\mp 1,0);(\mp 1,0,\mp 1);(0,\mp 1,\mp 1), & \alpha = 6..17 \\ (0,0,0), & \alpha = 18 \end{cases}$$

The discrete BGK equation and equilibrium distribution possess the form

$$f_i(\vec{x}+\vec{\xi}_i\delta t, t+\delta t) = f_i(\vec{x},t) + \omega\delta t(f_i^{\mathrm{eq}}(\vec{x},t) - f_i(\vec{x},t)),$$

$$f_i^{\mathrm{eq}}(\vec{x},t) = \rho t_{\mathrm{P}}\left[1 + \frac{\xi_{i,\alpha}u_\alpha}{c_{\mathrm{S}}^2} + \frac{u_\alpha u_\beta}{2c_{\mathrm{S}}^2}\left(\frac{\xi_{i,\alpha}\xi_{i,\beta}}{2c_{\mathrm{S}}^2} - \delta_{\alpha,\beta}\right)\right]$$

$\alpha = 1, 2, 3$ and $\beta = 1, 2, 3$ represent the space dimensions and $\delta_{\alpha,\beta}$ is the Kronecker delta. The coefficients t_{P} are weighting factors to be chosen such that macroscopic symmetry, conservation of mass and momentum are satisfied. For the D3Q19 model one obtains $t_0 = \frac{1}{3}$, $t_1 = \frac{1}{18}$, $t_2 = \frac{1}{36}$ and $c_{\mathrm{S}} = \frac{1}{\sqrt{3}}\delta x/\delta t$ where the index describes the square modulus of the discrete velocities ξ_i. To derive the weighting factors, see Succi (2001). The macroscopic flow values are determined by summation over the base moments

$$\rho = \sum_{i=1}^{i=i_{\max}} f_i = \sum_{i=1}^{i=i_{\max}} f_i^{\mathrm{eq}}$$

$$\rho u_\alpha = \sum_{i=1}^{i=i_{\max}} \xi_{\alpha,i} f_i = \sum_{i=1}^{i=i_{\max}} \xi_{\alpha,i} f_i^{\mathrm{eq}}$$

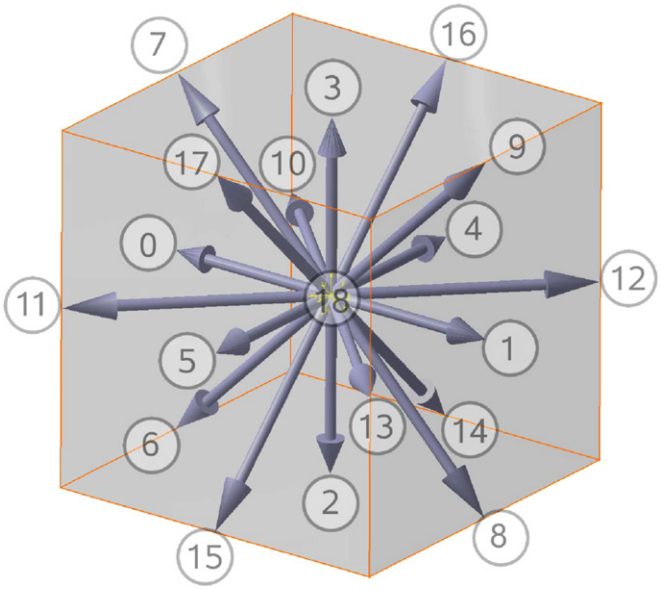

Fig. 1. The D3Q19 model.

The standard LBM describes weakly compressible flows. To further decouple the pressure and the density, i.e., to obtain a solution method for incompressible flows, a modified equilibrium distribution function is applied as proposed by Zou et al. (1995). The modified discrete equilibrium distribution reads

$$f_i^{\mathrm{eq}}(\vec{x},t) = t_{\mathrm{P}}\left[\rho + \frac{\xi_{i,\alpha}u_\alpha}{c_{\mathrm{S}}^2} + \frac{u_\alpha u_\beta}{2c_{\mathrm{S}}^2}\left(\frac{\xi_{i,\alpha}\xi_{i,\beta}}{2c_{\mathrm{S}}^2} - \delta_{\alpha,\beta}\right)\right]$$

All the results in this study are performed with the incompressible LBM–BGK method.

2.2. Boundary conditions and fluid properties

Three kinds of boundary conditions are applied, in and outflow velocity boundary conditions, fixed walls and zero pressure and velocity gradients. First, the formulation at inspiration is discussed. In Große et al. (2007), a fully developed laminar inflow was created by an artificial prolongation of the tracheal exit shape. To simulate a fully developed laminar flow a parabolic inflow profile based on the normal wall distances of the tracheal cross section was generated. Additionally, the shape of the inflow profile, which is illustrated in Fig. 2, is oriented normal to the tracheal cross section.

For the numerous outlets at the sixth generation of the bronchial tree a zero-gradient formulation of the macroscopic flow variables in the direction of the outlet is prescribed. At expiration the conditions for the trachea and the branches of the sixth generation are reversed.

To simulate no-slip boundary conditions an interpolated bounce-back scheme as proposed in Bouzidi et al. (2001) is implemented.

The dimensional fluid properties correspond to those of air at normal conditions, i.e., the density is $\rho = 1{,}225\,\mathrm{kg/m^3}$, the kinematic viscosity $\nu = 1.4\times10^{-5}\,\mathrm{m^2/s}$, and the temperature $T = 293\,\mathrm{K}$. The inlet mass flow is 360 ml/s at a hydraulic diameter-based $Re_{\mathrm{D}} = 1250$ with a mean inlet velocity $v = 0.972\,\mathrm{m/s}$. The hydraulic diameter D is defined as $D = 4A_{\mathrm{Trachea}}/U_{\mathrm{Trachea}}$, with A_{Trachea} being the tracheal inlet cross section and U_{Trachea} the circumference of the tracheal inlet cross section such that $D = 18.3\,\mathrm{mm}$ in the current analysis.

2.3. Computational grid

The model geometry for the flow simulation is based on a cast of the human lung including the larger part of the trachea down to the sixth generation of the bronchial tree. The same lung data was used to generate the model of the particle-image velocimetry (PIV) measurements performed in Große et al. (2007). The geometry of the stereolithography (STL) model is given in Fig. 3. The STL surface data obtained by a CT scan of the lung cast is the basis to generate the computational grid by an in-house automatic Cartesian grid generator. The complete model geometry is resolved with 18.6 million Cartesian grid cells.

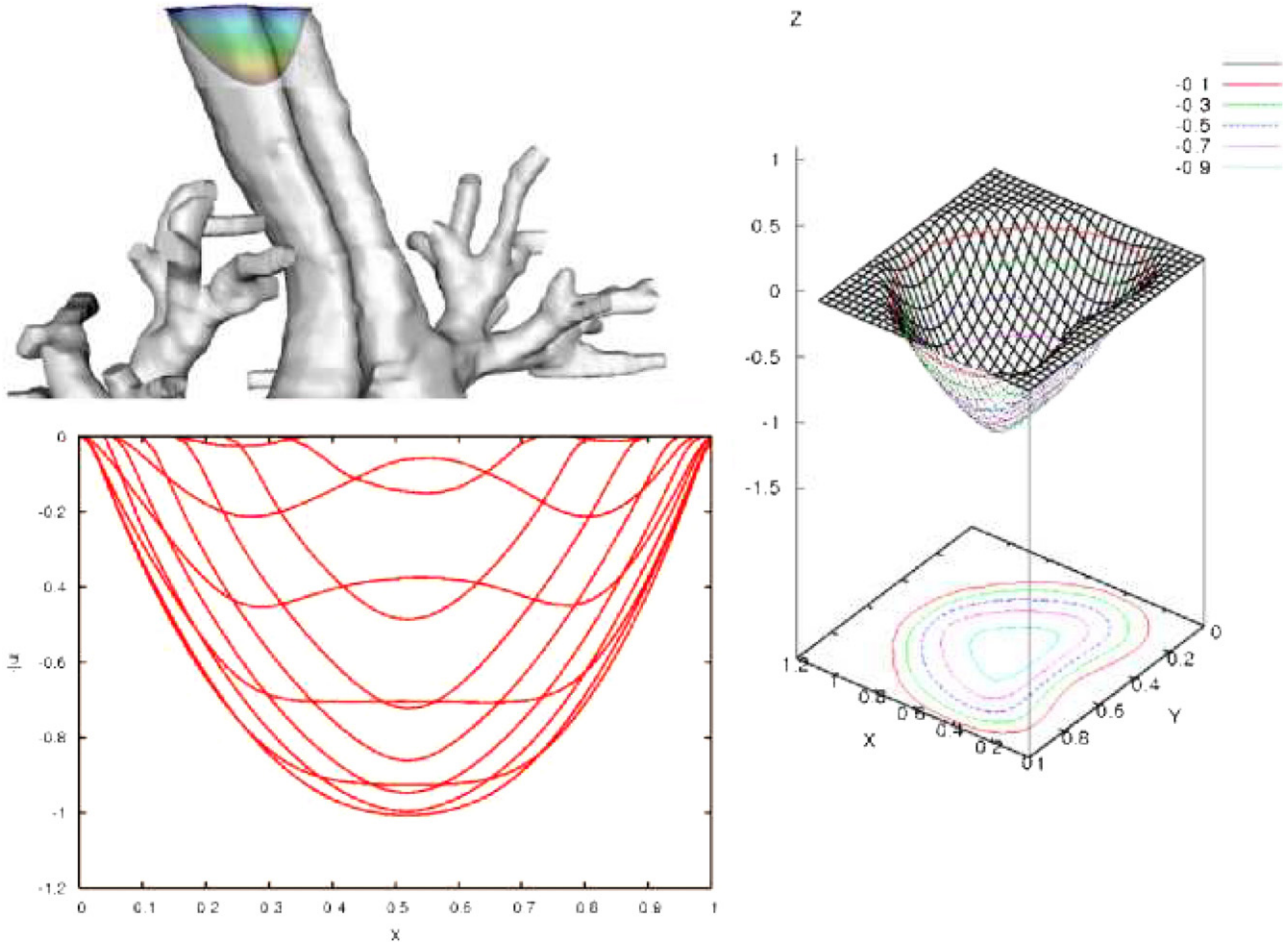

Fig. 2. Inflow velocity profile for inspiration. Inlet location (left top), normalized velocity profiles at various y-positions of the inlet (left bottom), three-dimensional normalized velocity profile with contour levels (right).

To ensure grid convergence calculations with three different resolutions, namely 8.0, 12.5 and 18.6 million cells, have been carried out. Fig. 4 shows the velocity magnitude in the center line of the reference plane given in Fig. 5. While the 8.0 million cell simulation has a higher maximum velocity magnitude the plots of the other two cases collapse. All simulations reach a steady state as is evidenced by the residuals of the density and velocity components which are between 10^{-12} and 10^{-14} in all cases.

The computations are performed with the above-described in-house lattice-Boltzmann solver on the JUMP cluster of the Jülich Supercomputing Center. The steady-state simulations for inflow and outflow each take <10 h. Furthermore, to generate the mesh based on the CT determined surfaces takes <2 h, which is much less than the overall time for the manual or semi-automatic grid generation of structured grid-based methods. For those methods the grid generation usually is the most time consuming part and takes days or weeks depending on the complexity of the grid. For model geometries with a similar degree of complexity like in this study the geometry usually has to be simplified before a manual grid generation can be considered.

3. Numerical–experimental comparison

Recently, it has been demonstrated that the flow field inside realistic geometries of the bronchial tree can be numerically simulated as shown by Ertbruggen et al. (2005) and Lin et al. (2007). Their simulations give further insight into the physical understanding of the flow patterns in the lungs. However, the numerical solution of flow fields in complex geometries is usually very sensitive to the boundary conditions, the grid resolution and overall algorithm. Therefore, a validation of the numerical results with experimental findings is essential to evidence the quality of the computed data.

To validate the numerical solutions, the velocity contours in the reference plane given in Fig. 6 for the steady flow case at $Re_D = 1250$ are compared with PIV measurements from Große et al. (2007). In this discussion two issues have to be kept in mind. First, the PIV data cannot be considered accurate in the very near-wall region due to faulty vectors and reflections in this area. Therefore, the reliable region has been marked by the black solid line in Figs. 7 and 8. Second, the data base of the PIV measurements is smaller than the numerical data set,

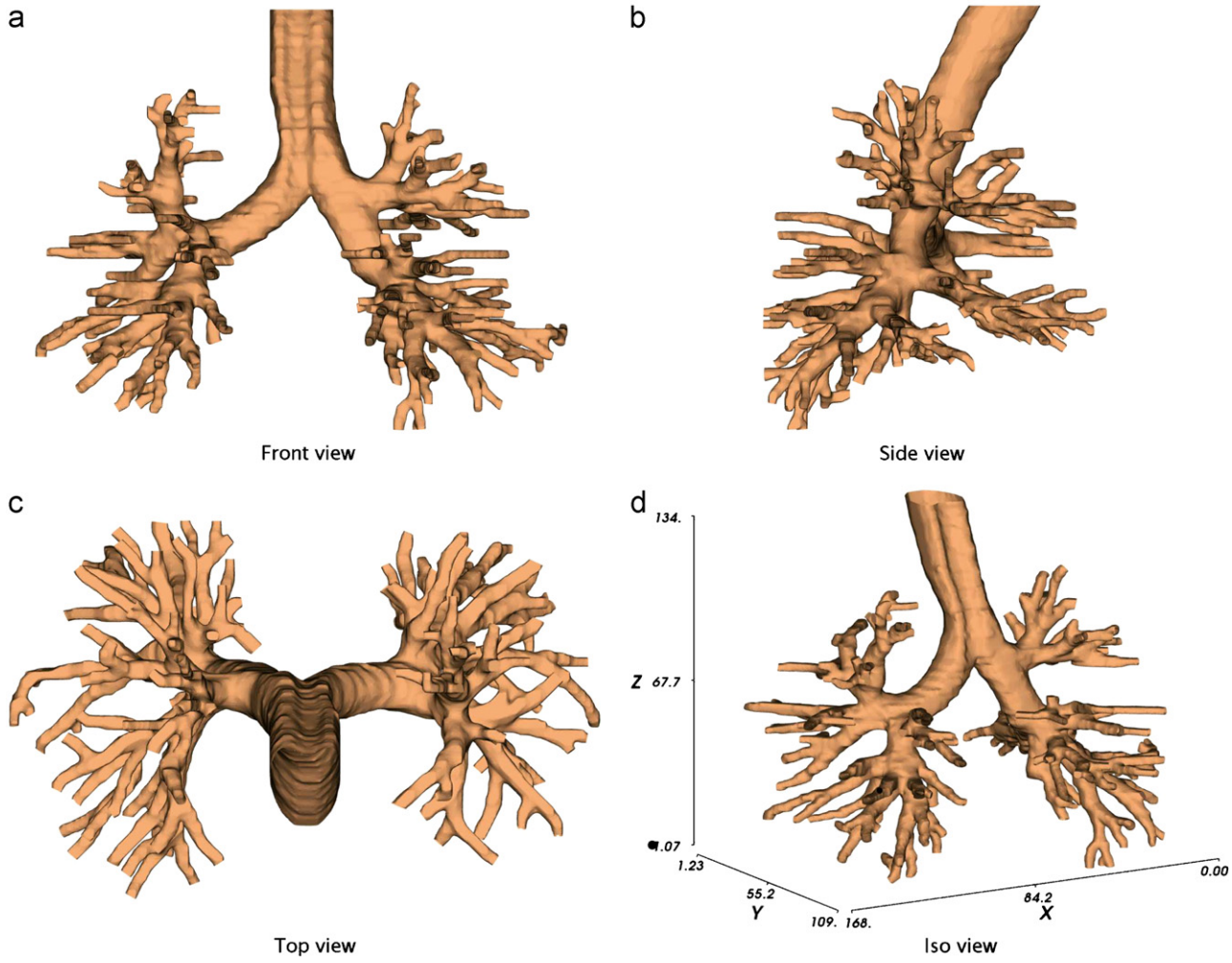

Fig. 3. Lung cast geometry.

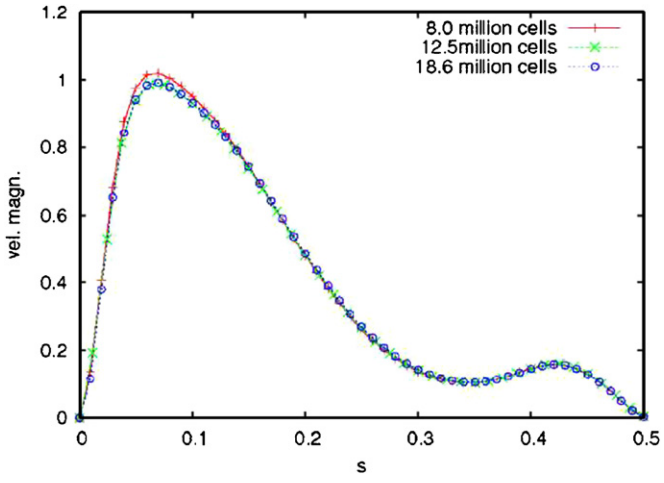

Fig. 4. Velocity magnitude on the center line s of a reference plane for three different grid resolutions.

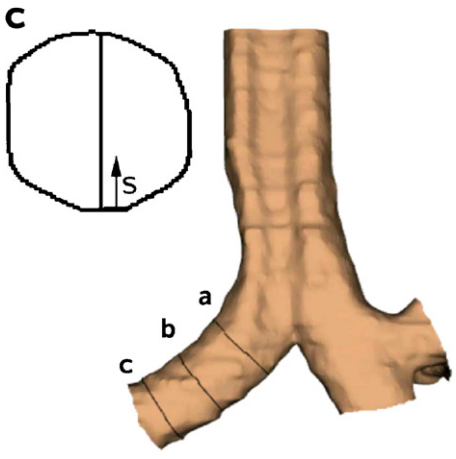

Fig. 5. Reference plane and center line s for the comparison of the velocity magnitudes.

resulting in a less smooth illustration of the color contours of the flow field.

The comparison of the velocity magnitude contours at inspiration in Fig. 7 shows good qualitative agreement between experiment and simulation. The decomposition of the mass flux in the left and right primary bronchus is very similar and the shape of the bulk velocity distribution in the tracheal section nearly coincides. The contours in the

region of lower velocity in the left primary bronchus, which indicate the secondary flow, are also in good agreement. The comparison of the peak velocity values in the various cross sections evidences even a convincing quantitative correspondence.

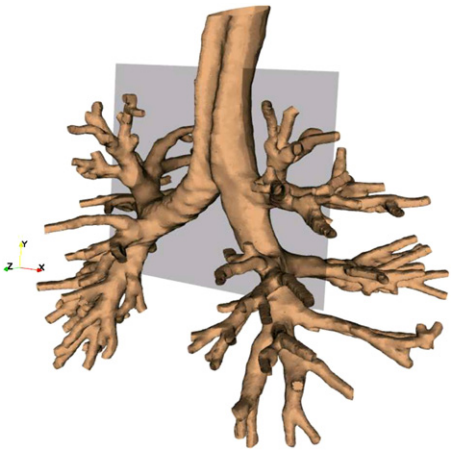

Fig. 6. Reference plane for comparison with PIV data.

At expiration the agreement of experimentally and numerically determined velocity contours in the tracheal and primary bronchi is still good, although the velocity in the bronchi is somewhat smaller in the simulation. The secondary flow in the tracheal section is more pronounced resulting in a less full velocity distribution in the numerical simulation than in the measurements. This slight difference is assumed to be due to the choice of the boundary conditions in the outlet cross sections of the highest generations of the bronchial tree. In the experimental setup, which is shown in Fig. 9 these outlets are connected to the tubes drilled in a silicon block in which the model resides. These tubes are not considered in the simulation. At inspiration their influence is much smaller than at expiration since the main impact of the perturbation generated on the boundary occurs in the mainstream direction. Furthermore, these drilled holes are only a necessity of the experimental setup and

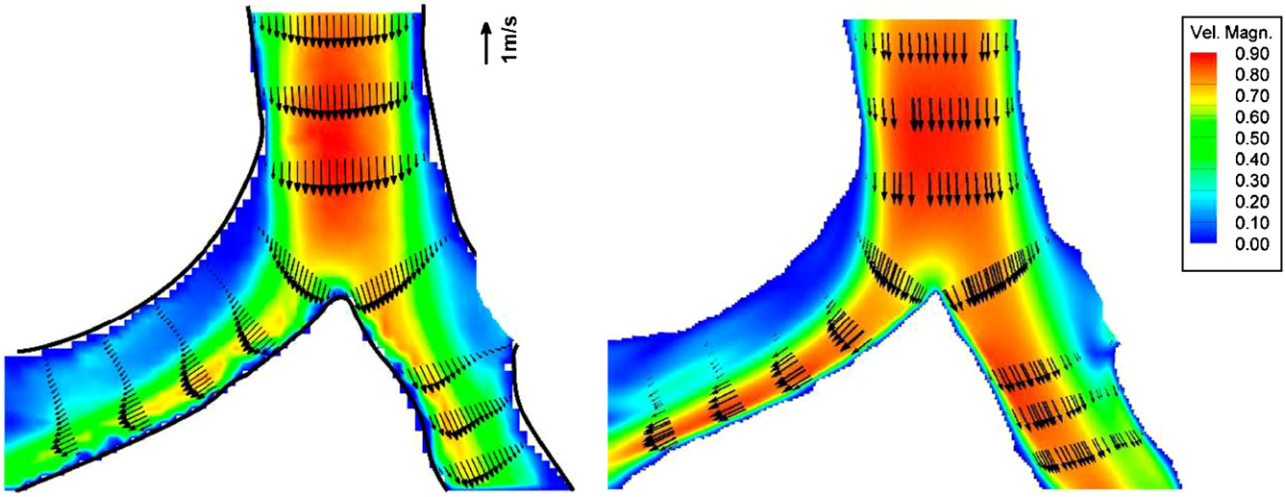

Fig. 7. Velocity contours and distributions at inspiration at $Re = 1250$; PIV (left), simulation (right).

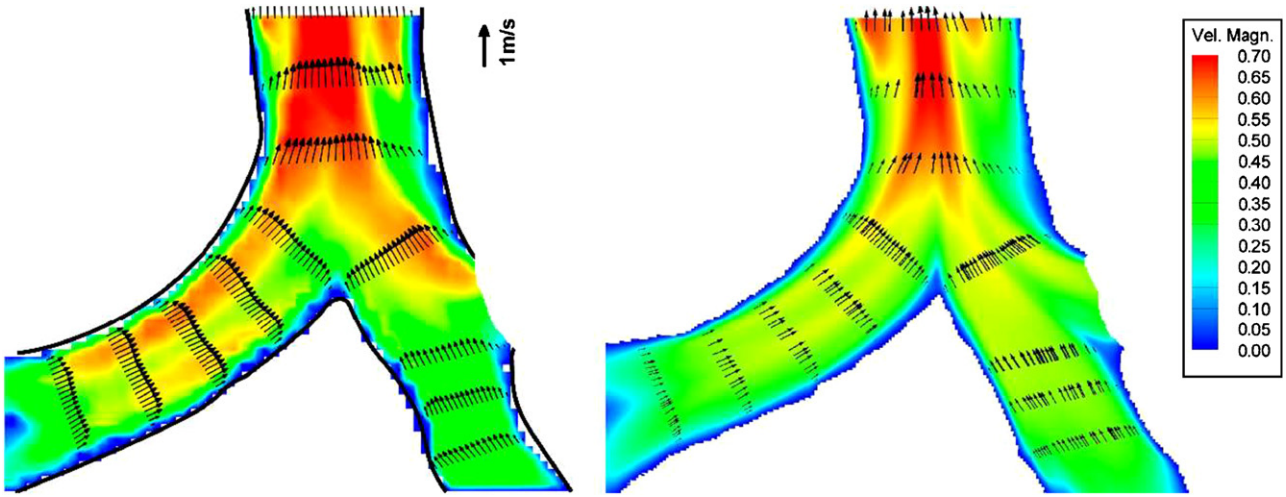

Fig. 8. Velocity contours and distributions at expiration at $Re = 1250$; PIV (left), simulation (right).

therefore, they are intentionally not included in our simulation.

The secondary flow structures at inspiration were also observed in other numerical findings like Zhang et al. (2002), Liu et al. (2003) and Ertbruggen et al. (2005) and in the experiment of Große et al. (2007), who investigated the flow details by measurements in several streamwise located planes, especially in the left primary bronchus. However, a complete illustration of the secondary vortex structures could not be gained in the investigated parallel planes. The current numerical simulation allows a detailed study of the secondary flow structures in the first bifurcation. Fig. 10 shows the numerically determined in-plane velocity distributions and contours at several cross sections in the left primary bronchus for two Reynolds numbers, $Re_D = 1250$ and 1700. The small differences in the velocity distributions and contours at the different Reynolds numbers shows the shape and orientation of the secondary vortices to be relatively independent of the Reynolds number in the investigated range and at steady inspiration. The shape of the counter-rotating vortices changes in the streamwise direction in the left principal bronchus. Fig. 10(a) shows that close to the bifurcation only the right vortex is clearly developed. Further downstream in Fig. 10(b) and (c) the left vortex develops resulting in a counter-rotating vortex structure which also was observed in Große et al. (2007). Unlike the experimental investigation this numerical analysis clearly shows the vortex pair to occur somewhat downstream of the bifurcation and their centers to be located extremely close to the upper wall. The lowest streamwise velocities are clearly observed in the upper part of cross section (a) in Fig. 10. It is in this area where particles are likely to be deposited.

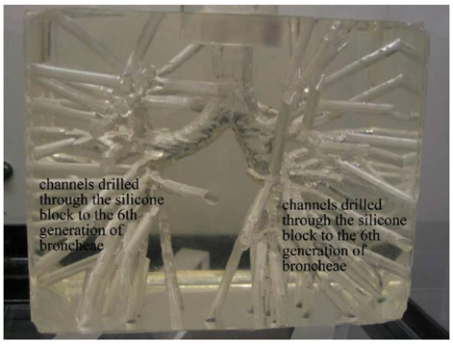

Fig. 9. Silicon lung of the experimental setup in Große et al. (2007).

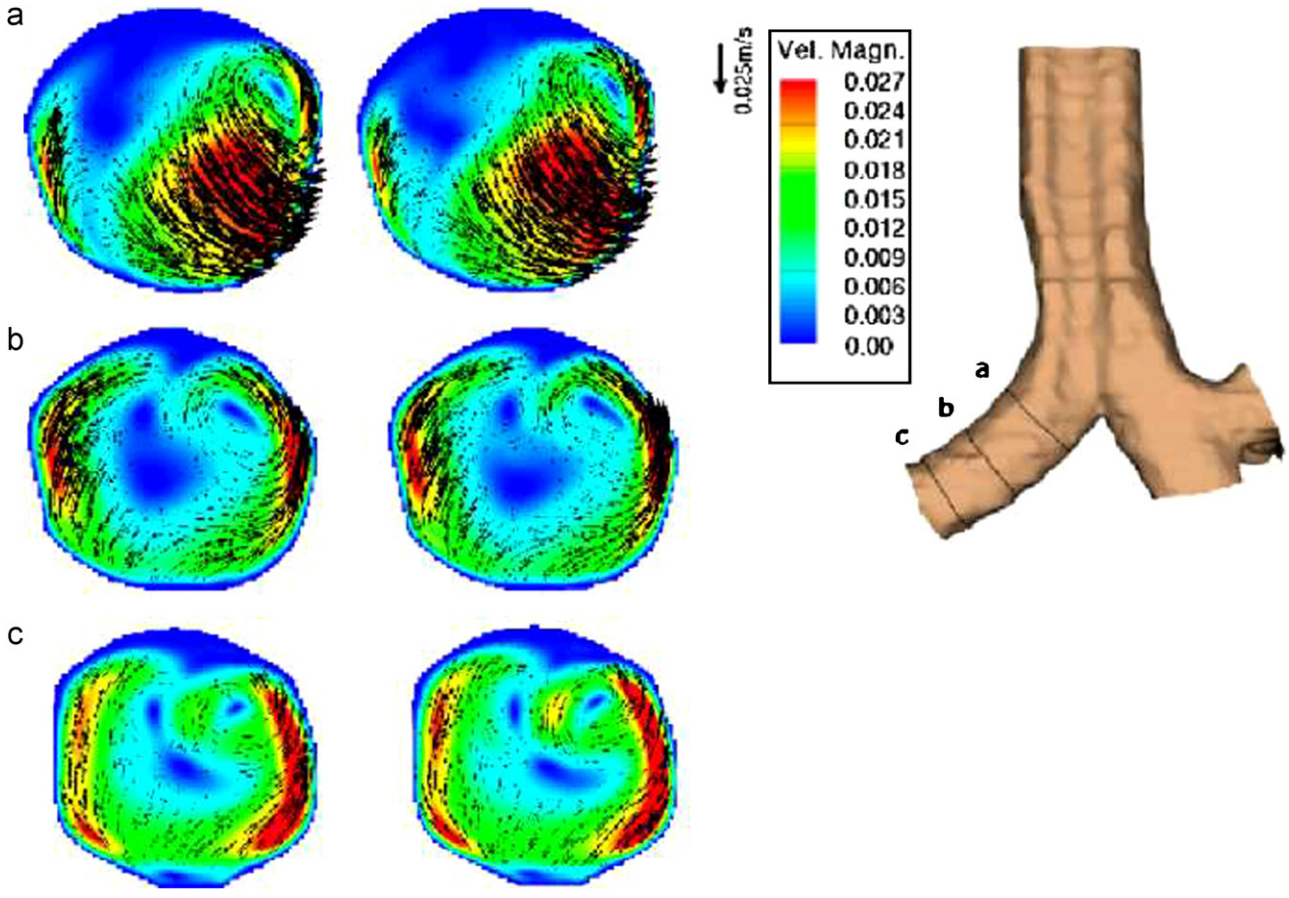

Fig. 10. In-plane velocity distributions and contours of the secondary flow structure at inspiration in the left primary bronchus for $Re = 1250$ (left) and $Re = 1700$ (right).

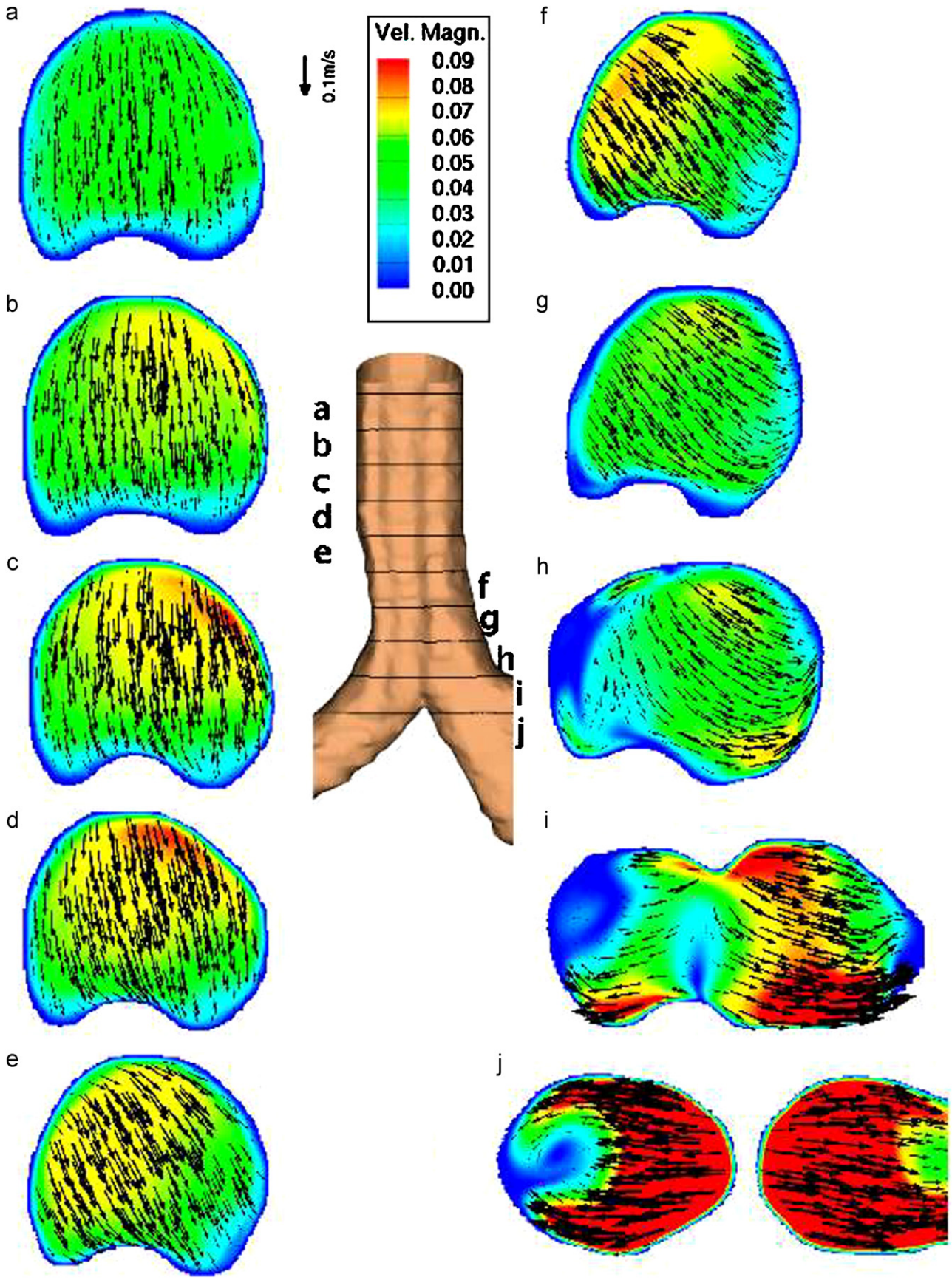

Fig. 11. In-plane velocity distributions and contours at $Re = 1250$ in several cross sections in the trachea at inspiration.

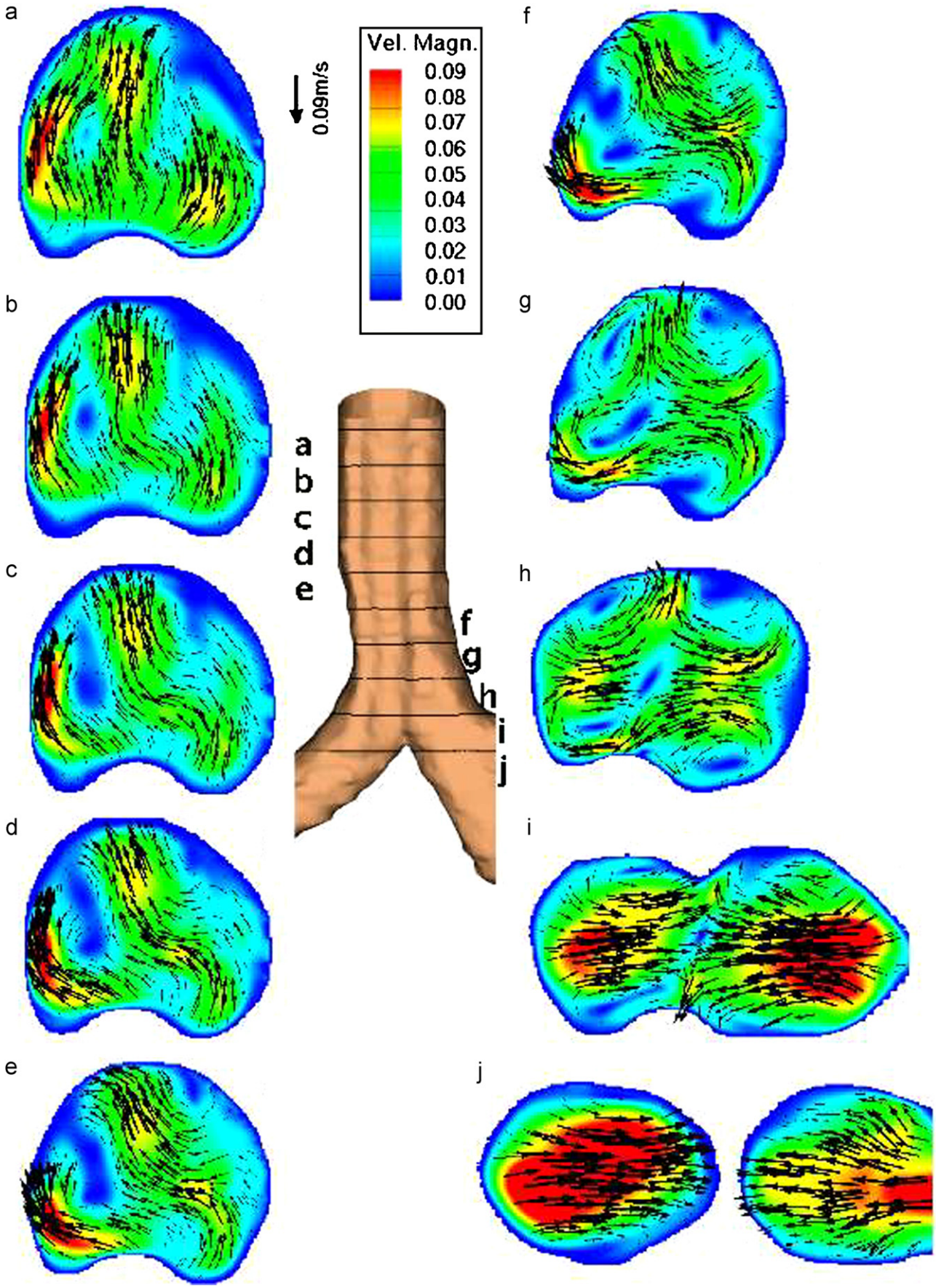

Fig. 12. In-plane velocity distributions and contours at $Re = 1250$ in several cross sections in the trachea at expiration.

4. Characteristic three-dimensional flow patterns at inspiration and expiration

In the following, first, the differences in the flow patterns in the trachea at steady inspiration and expiration are shown. Then, the relation between the tracheal flow pattern and the mass flux distribution in the higher bifurcations of the lung is discussed. To analyze the three-dimensional flow patterns in the tracheal section, the velocity distributions and contours in several cross sections have been investigated. Fig. 11(a)–(g) show the velocity distributions at inspiration to have a unique orientation in each cross section. In Fig. 11(h) the flow is split into two sub-branches and in Fig. 11(j) the onset of the secondary flow structure in the left principal bronchus can be observed.

The velocity field at steady expiration in Fig. 12 possesses a very intricate flow structure, unlike the velocity field at inspiration. These complex patterns in the trachea are a consequence of the asymmetric merging of the two air streams coming from the left and right principal bronchus. In Fig. 12(h) two counter-rotating vortex pairs are observed which meander and decay in the downstream direction (Fig. 12(f)–(a)). Note Fig. 12(j) evidences a full velocity distribution. That is, particles being deposited in this area at inspiration are expired. In other words, to make sure that particles reach higher bifurcation areas, it is necessary to circumvent this area of low velocity at inspiration.

To obtain a better understanding of the flow pattern in the lung and to relate origin and destination of the flow at inspiration and expiration streamlines were visualized and colored according to their starting and end loci, respectively. The results are shown in Figs. 13 and 14. The colors indicate the parts of the mass flux entering at inspiration and exiting at expiration the left principal bronchus (dark blue), the lower right bronchus (cyan) and the upper right bronchus (white). Fig. 13 shows a larger part of the near-wall flow to be inspired into the upper right lobar bronchus, while the center flow nearly evenly splits into the left principal bronchus and lower right bronchus. At expiration the tracheal positions of the streamlines exiting the right bronchi possess a highly complex distribution. That is the flow from the right upper bronchus streams into the center of the tracheal cross section and displaces the mass flux from the lower right bronchus. In addition, the streams from the right bronchi are interwoven, which excites the complex double counter-rotating vortex pair structures in Fig. 12.

This knowledge on the general air exchange processes in the upper human airways is essential for aerosolized drug delivery, since it allows exact drug delivery into certain parts of the bronchi, e.g. by using a tubus that surpasses the oral and nasal sections. Furthermore, the characteristic streamline patterns in cross sections of the trachea enable to detect small particles and relate their origin to defined locations of the lung at exhalation. Hence, a localized prognosis for defects of the bronchial tree is possible without examining the higher bifurcations.

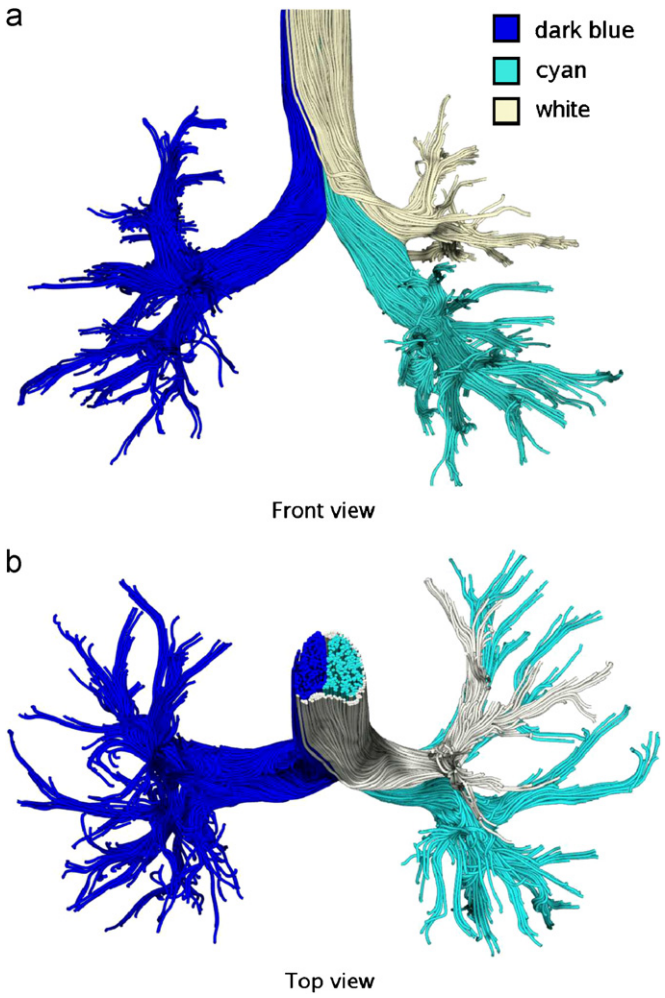

Fig. 13. Streamline patterns at steady inspiration.

5. Discussion

The flow field at steady inspiration and expiration inside a human lung has been simulated via the LBM.

The results have been compared with PIV measurements and showed the numerical solutions to be in very good agreement with the experimental findings. The secondary flow structures that have been observed in the experimental investigation of Große et al. (2007) have been captured and described in detail. Additionally, the three-dimensional flow with emphasis on the secondary flow in the trachea and the left and right principal bronchi has been analyzed. The investigation shows a clear flow decomposition in the trachea at inspiration and expiration which is related to the higher bifurcations. The analysis of the streamlines reveals a switching of the tracheal position of the air streams of the right upper and lower bronchus at expiration and inspiration. The knowledge of these flow patterns plays an important role to study aerosolized drug delivery processes and localized diagnostics of lung diseases.

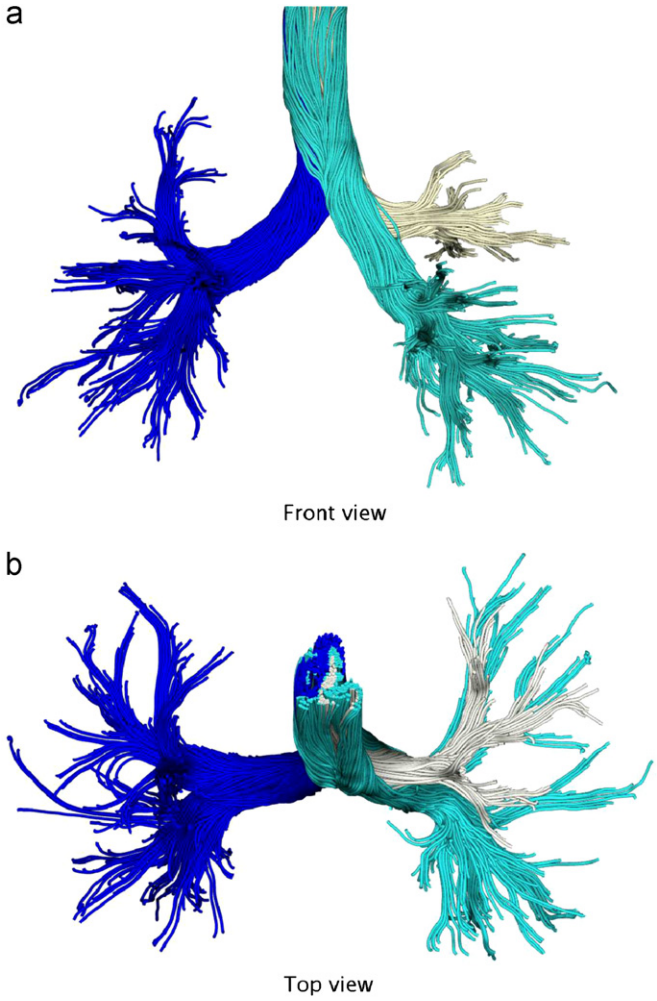

Fig. 14. Streamline patterns at steady expiration.

In all simulated cases a steady flow field throughout the complete simulation domain was recovered. It goes without saying that the application of steady boundary conditions for inspiratory and expiratory lung flow neglects several phenomena like the geometrical deformation of the bronchial tree and the temporal development of vortical flow structures in the lower generations of the bronchial tree. Furthermore, the effects of the laryngeal jet at inspiration as investigated by Kleinstreuer and Zhang (2003), Zhang and Kleinstreuer (2003) and Ball et al. (2007), cannot be recovered with the current choice of boundary conditions and geometry. Nonetheless, the physics concerning the trajectories discussed in this study can be assumed to describe the correct general flow phenomena for a large part of the breathing cycle when low breathing conditions, i.e., small Strouhal numbers are considered.

Furthermore, it can be expected that the described flow switching phenomenon in the trachea is also present, possibly even more pronounced, in the unsteady case. In brief, steady-state simulations can be considered appropriate to investigate basic flow phenomena in the lung, which are not dominated by the local time derivative of the velocity vector. If the temporal flow development and effects including the gas exchange between different subbranches, e.g., pendulum air are analyzed, unsteady flow simulations are necessary. Note, however, to accurately capture the real flow physics in a human lung, this also requires the temporal resolution of the moving geometry and the interaction of liquid and air in the sublayer covering the surface.

In other words, more research have to be done to fully investigate lung flow. The validity and physical impact of the switching phenomenon on HFV is currently investigated by unsteady flow simulations.

Future analyses will also include steady and unsteady particle decomposition studies and the simulation of the complete tracheal, oral, and nasal sections.

Conflict of interest

To the best of our knowledge there is no conflict of interest.

Acknowledgments

Most of the images were generated using the Paraview visualization software developed by Kitware, Sandia Labs and CSimSoft. The support of the Deutsche Forschungsgemeinschaft (DFG) for this research is gratefully acknowledged.

References

Ball, C.G., Udin, M., Pollard, A., 2007. Mean flow structures inside the human upper airway. Flow, Turbulence and Combustion (doi:10.1007/s10494-007-9113-3).

Bhatnagar, P.L., Gross, E.P., Krook, M., 1954. A model for collision processes in gases, I: small amplitude processes in charged and neutral one-component systems. Physics Review 94 (3), 511–519.

Boghosian, B.M., Yepez, J., Coveney, P., Wagner, A., 2001. Entropic lattice Boltzmann methods. Proceedings of the Royal Society of London Series A, 457(717).

Bouzidi, M., Firadaouss, M., Lallemand, P., 2001. Momentum transfer of a Boltzmann-lattice fluid with boundaries. Physics of Fluids 13 (11), 3452–3459.

Comer, J.K., Kleinstreuer, C., Zhang, Z., 2001. Flow structures and particle deposition patterns in double-bifurcation airway models. Part 1. Air flow fields. Journal of Fluid Mechanics 435, 25–54.

d'Humieres, D., Ginzburg, I., Krafczyk, M., Lallemand, P., Luo, L.S., 2002. Multiple-relaxation-time lattice Boltzmann models in three dimensions. Royal Society of London Philosophical Transactions Series A 360, 437–451.

Ertbruggen, C.V., Hirsch, C., Paiva, M., 2005. Anatomically based three-dimensional model of airways to simulate flow and particle transport using computational fluid dynamics. Journal of Applied Physiology 98, 970–980.

Finck, M., Hänel, D., Wlokas, I., 2007. Simulation of nasal flow by lattice Boltzmann methods. Computers in Biology and Medicine 37, 739–749.

Freitas, R.K., Schröder, W., 2008. Analysis of internal turbulent flow using lattice-Boltzmann methods, Computers and Fluids (under review).

Geier, M., Greiner, A., Korvink, J.G., 2006. Cascaded digital lattice Boltzmann automata for high Reynolds number flow. Physical Reviews E, 73(6) (doi:10.1103/PhysRevE.73.066705).

Geller, S., Krafczyk, M., Tölke, J., Turek, S., Hron, J., 2006. Benchmark computations based on lattice-Boltzmann, finite element and finite volume methods for laminar flows. Computers and Fluids 35, 888–897.

Große, S., Schröder, W., Klaas, M., Klöckner, A., Roggenkamp, J., 2007. Time resolved analysis of steady and oscillating flow in the upper human airways. Experiments in Fluids 42, 955–970.

Hänel, D., 2004. Molekulare Gasdynamik. Springer, Berlin.

Kleinstreuer, C., Zhang, Z., 2003. Laminar-to-turbulent fluid–particle flows in a human airway model. International Journal of Multiphase Flow 29, 271–289.

Li, Z., Kleinstreuer, C., Zhang, Z., 2007. Particle deposition in the human tracheobronchial airways due to transient inspiratory flow patterns. Journal of Aerosol Science 38, 625–644.

Lin, C., Tawhai, M.H., McLennan, G., Hoffmann, E.A., 2007. Characteristics of the turbulent laryngeal jet and its effect on airflow in the human intra-thoracic airways. Respiratory Physiology and Neurobiology 157, 295–309.

Liu, Y., So, R.M.C., Zhang, C.H., 2003. Modeling the bifurcating flow in an asymmetric human lung airway. Journal of Biomechanics 36, 951–959.

Nowak, N., Kakade, P.P., Annapragada, A.V., 2003. Computational fluid dynamics simulation of airflow and aerosol deposition in human lungs. Annals of Biomedical Engineering 31, 374–390.

Qian, Y.H., D'Humieres, D., Lallemand, P., 1992. Lattice BGK models for Navier–Stokes equation. Europhysics Letters 17 (6), 479–484.

Succi, S., 2001. The Lattice Boltzmann Equation for Fluid Dynamics and Beyond. Numerical Mathematics and Scientific Computation. Clarendon Press, Oxford.

Weibel, E.R., 1963. Morphometry of the Human Lung. Springer, Berlin.

Zhang, Z., Kleinstreuer, C., 2003. Low Reynolds number turbulent flows in locally constricted conduits: a comparison study. AIAA Journal 41, 831–840.

Zhang, Z., Kleinstreuer, C., Kim, C.S., 2002. Gas–solid two-phase flow in a triple bifurcation lung airway model. International Journal of Multiphase Flow 28, 1021–1046.

Zhao, Y., Lieber, B.B., 1994a. Steady inspiratory flow in a model symmetric bifurcation. Journal of Biomechanical Engineering 116, 488–496.

Zhao, Y., Lieber, B.B., 1994b. Steady expiratory flow in a model symmetric bifurcation. Journal of Biomechanical Engineering 116, 318–323.

Zou, Q., Hou, S., Chen, S., Doolen, G.D., 1995. An improved incompressible lattice Boltzmann model for time-independent flows. Journal of Statistical Physics 81, 35–49.